

Rotationally resolved spectra of the 4051 Å comet band of C₃ for all six ¹²C and ¹³C isotopologues



M.A. Haddad^a, D. Zhao^b, H. Linnartz^{b,a}, W. Ubachs^{a,*}

^a Department of Physics and Astronomy, LaserLab, VU University Amsterdam, De Boelelaan 1081, NL 1081HV Amsterdam, The Netherlands

^b Sackler Laboratory for Astrophysics, Leiden Observatory, University of Leiden, PO Box 9513, NL 2300 RA Leiden, The Netherlands

ARTICLE INFO

Article history:

Received 4 October 2013

In revised form 17 January 2014

Available online 27 January 2014

Keywords:

Cavity ring-down spectroscopy

Electronic spectroscopy

Carbon chain radicals

¹²C₃

C₃-isotopologues

ABSTRACT

Rotationally resolved absorption spectra of the $\tilde{A}^1\Pi_u-\tilde{X}^1\Sigma_g^+$ origin band of the tricarbon molecule (C₃) are reported for ¹²C₃ and its ¹³C-substituted isotopologues. The 4051 Å electronic transition, also identified in cometary tails and in translucent interstellar clouds, has been measured using cavity ring-down spectroscopy and a supersonically expanding planar plasma. Previous spectroscopic studies of ¹²C₃ are extended and the electronic origin band is re-investigated including a perturbation analysis of the upper state. The rotational analysis of spectra originating from ¹³C mono- and di-substituted C₃ yields accurate spectroscopic parameters for all six isotopologues, including ground state molecular constants for ¹³C¹²C¹³C and ¹²C¹³C¹³C.

© 2014 Elsevier Inc. All rights reserved.

1. Introduction

The tricarbon molecule (C₃) is an important intermediate in many chemical processes involving hydrocarbons. As one of the simplest linear centro-symmetric poly-atoms with a low resistance to bending, C₃ serves as a benchmark molecule in quantum chemistry and molecular physics [1,2]. The 4051 Å band of C₃ was first detected in cometary emission in 1881 [3] and later in the laboratory in 1942 [4]. In 1951 C₃ was unambiguously identified as the emitter of this band following a ¹³C-substitution experiment [5]. Later, Gausset et al. [6,7] assigned the spectrum as the $\tilde{A}^1\Pi_u-\tilde{X}^1\Sigma_g^+$ electronic transition based on a detailed rotational analysis of a number of vibronic bands. Due to the complexity of the spectrum, partly because of the existence of a low frequency bending mode, a large number of experimental and theoretical studies were needed to attain a comprehensive characterization of the $\tilde{A}^1\Pi_u-\tilde{X}^1\Sigma_g^+$ transition of C₃.

C₃ has also attracted long-term interest from astronomers because of its important role in the chemistry of the interstellar medium (ISM). This small molecule is potentially involved in the formation of more complex molecules such as carbon chains and carbonaceous circumstellar grains, and as a photo-fragment of polycyclic aromatic hydrocarbons (PAHs) [8,9]. Different from most asymmetric carbon-chain species, C₃ cannot be detected in the interstellar medium by radio astronomy due to the lack of a

permanent dipole moment. Detection of C₃ in circumstellar shells and in the dense ISM has been accomplished via ro-vibrational transitions in the mid- and far-infrared regions [10–13]. These detections prompted further high-resolution infrared laboratory studies [14–16] providing accurate molecular data for the electronic ground state.

The presence of C₃ in the diffuse ISM was first reported in 2001 [17], based on the detection of the 4051 Å band in the line of sight towards three reddened stars. Detection of C₃ in translucent clouds was then extended to several additional objects [18–21], all via the 4051 Å band. Recently, also a large set vibronic bands of the $\tilde{A}^1\Pi_u-\tilde{X}^1\Sigma_g^+$ system have been observed in diffuse clouds towards three reddened stars [22]. Up to now C₃ is the largest carbon chain molecule unambiguously identified in the diffuse ISM.

Spectroscopic studies of the $\tilde{A}^1\Pi_u-\tilde{X}^1\Sigma_g^+$ system of C₃ have thus far focused on the main isotopologue, ¹²C₃ [6,23–26]. Detailed laboratory investigations of the $\tilde{A}^1\Pi_u-\tilde{X}^1\Sigma_g^+$ 000–000 band of ¹²C₃ have revealed a complex perturbation phenomenon in the origin band. Several perturber lines in the $\tilde{A}^1\Pi_u$ 000 state of ¹²C₃ were found by McCall et al. [23] in laboratory work and later explained in a perturbation model by Zhang et al. [24]. However, the recent observation of a high resolution spectrum towards HD 169454 indicates that this model still does not fully explain the astronomically observed line intensities in the origin band [22].

Only a few laboratory studies have been performed on ¹³C-substituted C₃. The first spectroscopic study was performed by Douglas in 1951, determining the position of six band heads of isotopologue transitions corresponding with the 4051 Å band [5].

* Corresponding author.

E-mail address: w.m.g.ubachs@vu.nl (W. Ubachs).

In a subsequent study a tentative analysis of the rotationally resolved spectrum of pure $^{13}\text{C}_3$ was performed by Clusius and Douglas [27]. To our knowledge, no other spectroscopic work of the $\tilde{A}^1\Pi_u-\tilde{X}^1\Sigma_g^+$ electronic transition of $^{13}\text{C}_3$ has been reported. Other high-resolution studies of the fully ^{13}C substituted as well as mono-substituted $^{12}\text{C}^{12}\text{C}^{13}\text{C}$ and $^{12}\text{C}^{13}\text{C}^{12}\text{C}$ focused on vibrational transitions and have been performed in the mid-infrared region [28–30].

In this paper we present a systematic optical study of the 4051 Å band of all six isotopologues of C_3 . The $\tilde{A}^1\Pi_u-\tilde{X}^1\Sigma_g^+$ 000–000 band of $^{12}\text{C}_3$ is revisited, focusing on an experimental clarification of the rotational line intensities, and an extended Hamiltonian is presented to reproduce both transition frequencies and line intensities. High-resolution spectra of all five partially and fully ^{13}C substituted C_3 isotopologues are presented and analyzed, resulting in a set of molecular constants characterizing the $\tilde{A}^1\Pi$ upper electronic state. Moreover, for the ^{13}C di-substituted species the ground state constants are presented for the first time.

2. Experimental

In the present work, jet-cooled C_3 radicals and ^{13}C -substituted isotopologues are produced in a supersonically expanding planar plasma by discharging a mixture of acetylene in helium and argon. Mixtures of 0.5% $^{12}\text{C}_2\text{H}_2$ and 0.2% $^{13}\text{C}_2\text{H}_2$ diluted in He/Ar $\sim 1:1$ gas are used to generate $^{12}\text{C}_3$ and $^{13}\text{C}_3$ radicals, respectively. To study the partially ^{13}C -substituted C_3 isotopologues, i.e., $^{13}\text{C}^{12}\text{C}^{12}\text{C}$, $^{13}\text{C}^{12}\text{C}^{13}\text{C}$, $^{12}\text{C}^{13}\text{C}^{12}\text{C}$ and $^{12}\text{C}^{13}\text{C}^{13}\text{C}$, two ($^{12}\text{C}_2\text{H}_2 + ^{13}\text{C}_2\text{H}_2$)/He/Ar mixtures with a total acetylene concentration of $\sim 0.1\%$, and different $^{12}\text{C}:^{13}\text{C}$ isotope ratios of $\sim 2:1$ and $\sim 1:2$ are used. The gas mixture with a backing pressure of $\sim 5\text{--}9$ bar is supersonically expanded through a 30 mm \times 300 μm slit discharge nozzle into a vacuum chamber, which is evacuated by a roots blower pump station (1000 m^3/h). A ~ 300 μs negative high voltage pulse is applied to an expanding gas pulse, typically with $V/I \approx -500$ V/30 mA. Further details of the experimental setup and the operation of the pulsed slit discharge are described in Refs. [31,32].

The discharge nozzle is positioned in the vacuum chamber with its slit throat parallel to and ~ 5 mm downstream from the optical axis of a high finesse cavity consisting of two high reflectivity mirrors (Layertec, reflectivity $\sim 99.91\%$ at 405 nm). The optical cavity is used for cavity ring-down spectroscopy measurements. Tunable violet light at ~ 405 nm is generated by frequency-doubling the near infrared output (~ 810 nm) of a Nd:YAG (532 nm) pumped pulsed dye laser (Sirah, Cobra-Stretch) in a DKDP crystal. Light leaking out of the cavity is detected by a photomultiplier tube to record the ring-down decays. Typical ring-down times are $\sim 4\text{--}5$ μs . The experiment runs at a repetition rate of 8 Hz.

The non-linear scanning of the fundamental dye laser frequency is corrected by simultaneously recording the transmission fringes of two solid etalons (with free spectral ranges (FSR) ~ 20.1 and 7.57 GHz, respectively). The absolute frequency of the experimental spectra is calibrated by the Ar I line [33] at 24656.8325 cm^{-1} recorded through the plasma. The frequencies of isolated rotational transitions in the spectra are determined from Gaussian fits, while the overlapping line envelopes, abundantly present in spectra of the mixed isotopologues, are deconvoluted to obtain the transition frequencies. A comparison of the ground state combination differences of four isotopologues ($^{12}\text{C}_3$, $^{12}\text{C}^{12}\text{C}^{13}\text{C}$, $^{12}\text{C}^{13}\text{C}^{12}\text{C}$ and $^{13}\text{C}_3$) available from previous mid-infrared data and our spectra, shows that the relative accuracy with which frequencies can be determined is better than 0.04 cm^{-1} for spectral lines.

From the measurements of the fringe profile of the high-finesse etalon (FSR ~ 7.57 GHz), the bandwidth of the near infrared fundamental beam from the dye laser is estimated to be less than

0.03 cm^{-1} . The bandwidth of the violet light after frequency doubling is found to be ~ 0.07 cm^{-1} , estimated from the width of the narrowest feature (FWHM) in the final experimental spectra. Since the laser bandwidth is larger than the Doppler width – estimated at 0.03 cm^{-1} for the used expansion settings – effects on the experimental intensity patterns are expected [23]. In brief, under such conditions, the resonant fraction within the laser bandwidth profile will exhibit a more rapid decay of the ring-down transient due to absorption, while the non-resonant fraction within the laser bandwidth profile will experience decays of an empty cavity without absorption. Overall, this phenomenon results in non-exponential decay transients of the ring-down signal. As a consequence the differences in decay transients cannot be straightforwardly interpreted in terms of optical depth, and the line intensities in the recorded CRDS spectra become (to some extent) unreliable. This effect is relatively small for weak absorptions but becomes pronounced in the case of strong absorptions [34]. Therefore, in the present work, the $\tilde{A}^1\Pi_u-\tilde{X}^1\Sigma_g^+$ origin band of $^{12}\text{C}_3$ has been recorded for two different sets of experimental conditions in order to interpret the line intensity pattern correctly: one was aimed at obtaining the best signal-to-noise ratio (S/N), and consequently the largest number of weak transitions; the other was aimed at obtaining the most reliable line intensities of the strong low- J transitions.

3. Results and discussion

3.1. $^{12}\text{C}_3$

3.1.1. Rotational line intensities

The recorded absorption spectrum of $^{12}\text{C}_3$, shown in Fig. 1(a), has been recorded under plasma conditions as described in Ref. [31], i.e., ~ 10 bar backing pressure and $V/I \sim -750$ V/100 mA. The intensity pattern of this spectrum suffers significantly from the laser-bandwidth effect, similarly as in the spectra reported in Ref. [21]. An improved S/N in the present CRD experiment, though, makes it possible to observe more spectral features in the P-, Q- and R-branches. Many of the transitions in Fig. 1(a), which were assigned to perturbing states by Zhang et al. [24], show line intensities of almost equal magnitude compared to the regular (non-perturbed) transitions in the $\tilde{A}^1\Pi_u-\tilde{X}^1\Sigma_g^+$ system. Monitoring the ring-down decay signal during the spectral recordings, confirms that for most absorption lines in this region, the ring-down decays appear non-exponential [34].

As described above, the laser-bandwidth and non-exponential decay effects depend on the absorption depth and are considerably smaller for the weaker absorptions [34]. In order to achieve conditions guaranteeing reliable line intensities, it is necessary to control the C_3 radical density in the plasma, i.e., keeping the absorbance low, and therefore to reduce effects that lead to intensity anomalies. Similarly as in the study by McCall et al. [23], we recorded the spectra by confining the fit to the early part (3–4 μs) of each ring-down decay. This procedure, however, resulted in a comparable spectral pattern, but with a somewhat lower signal-to-noise ratio. Therefore we also varied the experimental settings for discharge power and precursor backing pressure. Fig. 1(b) shows the $^{12}\text{C}_3$ spectrum recorded for substantially different plasma conditions – $V/I \sim -400$ V/20 mA (estimated) and ~ 7 bar backing pressure – approaching the threshold conditions for generating a stable plasma in our experiment. The spectrum has a different pattern from the one shown in Fig. 1(a). This method, through discharge control, seems to be suitable for providing reliable estimates of the rotational line strengths. The resulting set of relative intensities for rotational line features, in part repre-

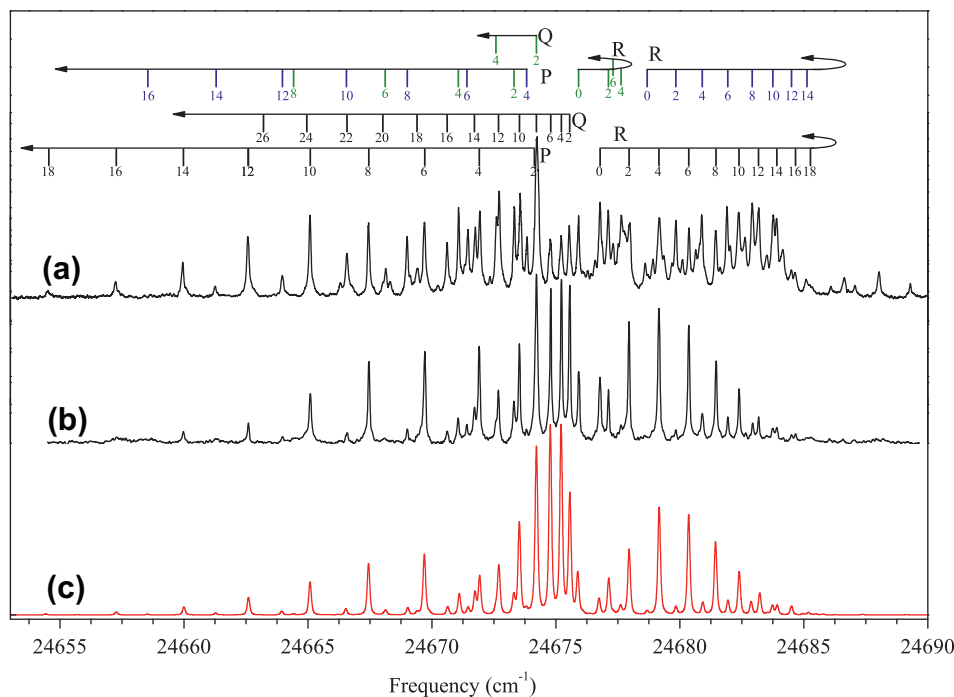


Fig. 1. Rotationally resolved spectra of the $\tilde{A}^1\Pi_u-\tilde{X}^1\Sigma_g^+$ electronic origin band of $^{12}\text{C}_3$. (a) Saturated spectrum recorded under high power discharge conditions with partially saturated line intensities; (b) Spectrum recorded under controlled discharge conditions preventing line saturation; (c) The red trace shows the simulated spectrum using a $^1\Pi_u-^1\Sigma_g^+$ Hamiltonian and with a Lorentzian line width of 0.07 cm^{-1} , a Gaussian line width of $\sim 0.1\text{ cm}^{-1}$, and with an estimated rotational temperature of $\sim 35\text{ K}$. Rotational transitions to perturber states $^3\Sigma_u^-$ and $P=1$ states are indicated with blue and green lines, respectively. (For interpretation of the references to color in this figure legend, the reader is referred to the web version of this article.)

sented in the spectrum of Fig. 1(b), can be reliably compared with a recently observed absorption spectrum of C_3 in a translucent cloud towards HD 169454 [22]. The astronomically derived rotational temperature ($\sim 21\text{ K}$ for low- J levels) is close to the actual rotational temperature in the supersonic jet in the present study.

The $^{12}\text{C}_3$ spectrum, shown in Fig. 1, comprises the main P, Q and R branches of the $\tilde{A}^1\Pi_u-\tilde{X}^1\Sigma_g^+$ 000–000 band and isolated absorption features that are likely due to other transient hydrocarbons in the plasma. The latter are often found in plasma expansions, as several species are formed simultaneously [35,36]. Some weak lines are due to ^{13}C mono-substituted C_3 isotopologues, observed in natural abundance, which is confirmed by the ^{13}C -substitution experiments that are discussed later.

3.1.2. The effective Hamiltonian for the $\tilde{A}^1\Pi_u$ (000) state of $^{12}\text{C}_3$

Only transitions starting from even- J levels in the ground state are observed for $^{12}\text{C}_3$, due to spin statistics. The line positions of the $\tilde{A}^1\Pi_u-\tilde{X}^1\Sigma_g^+$ 000–000 band of $^{12}\text{C}_3$ measured in this work are listed in Table 1. The transition frequencies agree well, i.e., within their experimental uncertainties with those previously reported by Zhang et al. and Tanabashi et al. [24,25].

The $\tilde{A}^1\Pi_u-\tilde{X}^1\Sigma_g^+$ electronic origin band of $^{12}\text{C}_3$ was found to be perturbed by Gausset et al. [7]. A number of extra lines were observed in a high-resolution laboratory study by McCall et al. [23], and later these features were ascribed to two long-lived perturber states, based on a time-delayed laser-induced fluorescence study by Zhang et al. [24]. In Ref. [24], an effective Hamiltonian was proposed for the upper $\tilde{A}^1\Pi_u$ state including two perturbing states (a $^3\Sigma_u^-$ state, and a $P=1$ vibronic state with regular P -type splittings) to reproduce all experimentally observed transition frequencies. Recent astronomical data and the new data presented here show a small mismatch with the calculated transition frequencies when using the Hamiltonian model given in Ref. [24]. Therefore, we introduce a similar Hamiltonian model as previously used but ex-

tended with matrix elements as given in Table 2. In this model, the Hamiltonian for the $\tilde{A}^1\Pi_u$ state and $P=1$ perturber state is defined as given in the Pgopher software [38]:

$$\mathbf{H}_{\Pi} = T_0 + (B \pm q/2)\mathbf{N}^2 - \mathbf{D}\mathbf{N}^4 + \mathbf{H}\mathbf{N}^6 \quad (1)$$

which results in the energy levels as:

$$E(J) = T_0 + (B \pm q/2)[J(J+1) - K^2] - \mathbf{D}[J(J+1) - K^2]^2 + \mathbf{H}[J(J+1) - K^2]^3 \quad (2)$$

where $K=1$ for the $\tilde{A}^1\Pi_u$ and $P=1$ perturber state. The '+' and '-' before the parameter q , refer to the levels with e and f parity, respectively, opposite to the definition in Refs. [6,24,25]. Moreover, it should be noted that the rotational term in Eq. (2) is expressed differently from the term used in Refs. [6,24,25], where

$$E(J) = T_0 + (B \pm q/2)J(J+1) - \mathbf{D}J^2(J+1)^2 + \mathbf{H}J^3(J+1)^3 \quad (3)$$

was used. The conversion factors between the molecular constants in Eqs. (2) and (3) are available from Table 4 of Ref. [39].

We start our perturbation analysis using a similar Hamiltonian matrix as described in Ref. [24]. The Hamiltonian matrix as used in the Pgopher software is given in Table 2. In the same way as in Ref. [24], we assume that the $P=1$ perturber state has a regular P -type splitting, described by a parameter q , while the spin-rotation interaction in the $^3\Sigma_u^-$ perturber state is neglected (γ fixed to 0). A least squares fit is made using Pgopher and the line list in Table 1 as input with exclusion of the two Q(2) lines that cause large residuals. The fit results in a set of molecular parameters very similar to those given in Ref. [24], although the parameters for $K=1$ states ($\tilde{A}^1\Pi_u$ state and $P=1$ perturber state) correspond to different definitions. To better describe the low- J levels in the upper $\tilde{A}^1\Pi_u$ state, the effective Hamiltonian model is adapted as follows:

Table 1
The frequencies (in cm^{-1}) and assignments of observed rotational lines in the $\tilde{A}^1\Pi_u-\tilde{X}^1\Sigma_g^+$ 000–000 band and transitions to perturber states in the electronic spectrum of $^{12}\text{C}_3$, and residuals from the fit (see text).

J''	Upper state	P-branch		Q-branch		R-branch	
		Obs.	$o-c$	Obs.	$o-c$	Obs.	$o-c$
0	$\tilde{A}^1\Pi_u$					24676.78	0.04
	$^3\Sigma_u^-$ ($P=1$)					24678.68	0.02
2	$\tilde{A}^1\Pi_u$	24674.13	-0.02	24675.56	-0.01	24675.92	0.04
	$^3\Sigma_u^-$ ($P=1$)					24677.95	-0.01
4	$\tilde{A}^1\Pi_u$	24673.31	0.01	24674.22	0.01	24677.12	-0.01
	$^3\Sigma_u^-$ ($P=1$)	24671.06	-0.04	24672.58	0.00	24677.63	0.02
6	$\tilde{A}^1\Pi_u$	24669.71	0.01	24674.79	0.02	24680.36	0.00
	$^3\Sigma_u^-$ ($P=1$)	24671.41	-0.05			24681.94	-0.01
8	$\tilde{A}^1\Pi_u$	24668.12	-0.02			24677.31	-0.01
	$^3\Sigma_u^-$ ($P=1$)	24667.46	0.01	24674.22	0.00	24681.46	0.02
10	$\tilde{A}^1\Pi_u$	24669.01	-0.02			24682.91	0.03
	$^3\Sigma_u^-$ ($P=1$)	24665.09	0.01	24673.53	0.00	24682.39	0.00
12	$\tilde{A}^1\Pi_u$	24666.55	0.02			24683.75	0.01
	$^3\Sigma_u^-$ ($P=1$)	24662.60	0.00	24672.68	-0.02	24683.18	-0.04
14	$\tilde{A}^1\Pi_u$	24663.98	0.03			24684.51	0.00
	$^3\Sigma_u^-$ ($P=1$)	24659.98	-0.02	24671.72	-0.02	24683.92	0.01
16	$\tilde{A}^1\Pi_u$	24661.30	0.02			24685.13	-0.05
	$^3\Sigma_u^-$ ($P=1$)	24657.27	0.01	24670.61	-0.02	24684.66 ^a	0.18
18	$\tilde{A}^1\Pi_u$	24658.54	0.01				
	$^3\Sigma_u^-$ ($P=1$)	24654.55 ^a	0.15	24669.40	0.00	24685.27 ^a	0.33
20	$\tilde{A}^1\Pi_u$	24651.73 ^a	0.30	24668.02	-0.02		
22	$\tilde{A}^1\Pi_u$			24666.57	0.02		
24	$\tilde{A}^1\Pi_u$			24664.95	0.02		
26	$\tilde{A}^1\Pi_u$			24663.20	0.00		

^a Transitions not included in the fit.

Table 2
Matrix for a perturbation analysis of the rotational level structure of the $\tilde{A}^1\Pi_u$ state and its perturbing states for $^{12}\text{C}_3$.

	$ \tilde{A}^1\Pi_u, f/e\rangle$	$ P=1, f/e\rangle$	$ ^3\Sigma_u^-, f/e\rangle$
$\langle\tilde{A}^1\Pi_u, f/e $	\mathbf{H}_{Π}^a	a	$\zeta(\mathbf{L}\cdot\mathbf{S})^b$
$\langle P=1, f/e $		\mathbf{H}_{Π}^a	0
$\langle^3\Sigma_u^-, f/e $	Symmetric		\mathbf{H}_{Σ}^c

^a The standard \mathbf{H}_{Π} for $^1\Pi$ or $P=1$ state is described by Eq. (1) in the text.

^b This term is set to affect e levels only, and is to be understood in terms of single-electron operators [37].

^c The standard \mathbf{H}_{Σ} for $^3\Sigma_u^-$ is expressed as [38]:
 $T_0 + B\mathbf{N}^2 + (2/3)\lambda(3S_z^2 - \mathbf{S}^2) + \gamma(\mathbf{N}\cdot\mathbf{S})$.

(a) In Ref. [24], the spin-rotation interaction in the perturber $^3\Sigma_u^-$ state is neglected, and a significant spin-spin interaction ($\lambda_{ss} \sim -7 \text{ cm}^{-1}$) results. Although the nature of this $^3\Sigma_u^-$ perturber state is still unclear, the large spin-spin interaction used here is difficult to explain, as it is more than four times larger than the spin-spin splitting in atomic carbon ($\sim 1.5 \text{ cm}^{-1}$), and also largely differs from the values in the $\tilde{a}^3\Pi_u$ and $\tilde{b}^3\Pi_g$ states of C_3 [40], as well as that in the $\tilde{b}^3\Sigma_g^-$ state of C_2 . Based on these considerations, we decided to fix $\lambda_{ss} \sim -0.1 \text{ cm}^{-1}$ in our analysis, close to the previously reported values for triplet C_3 and C_2 [40,41].

(b) The spin-rotation interaction is considered to be significant, and is explicitly included in our fit. As discussed in Ref. [24], the $^3\Sigma_u^-$ perturber may be a high vibronic level of the $\tilde{a}^3\Pi_u$ or $\tilde{b}^3\Pi_g$ state. In this case, as discussed in Ref. [42], the spin-

Table 3
Effective constants (in cm^{-1}) derived from a least-squares fit for the $\tilde{A}^1\Pi_u-\tilde{X}^1\Sigma_g^+$ electronic origin band of $^{12}\text{C}_3$.

		This work ^a	Ref. [24]	Ref. [25]
$\tilde{X}^1\Sigma_g^+$	B	0.4305883 ^b		0.4305883(58)
	$D \times 10^6$	1.437 ^b		1.437(13)
	$H \times 10^{10}$	1.129 ^b		1.129(35)
$\tilde{A}^1\Pi_u$	T_{00}	24675.489(14)	24675.632(80) ^c	24674.969(13) ^d
	B	0.412586(77)	0.41261(30) ^c	0.412632(23) ^d
	$D \times 10^6$	0.519 (fixed)	0.298 (fixed)	0.519(18) ^d
	$H \times 10^{11}$	5.35 (fixed)		5.35(43) ^d
	q	0.00023(16)	0.00125(59) ^d	0.0002906(16) ^d
$^3\Sigma_u^-$	T_{00}	24678.526(24)	24682.12(74)	
	B	0.42039(43)	0.4411(32)	
	$D \times 10^6$	1.0 (fixed)	-	
	λ	-0.1 (fixed)	-7.22(132)	
	γ	0.6093(70)	-	
$P=1e$	ζ	0.661(29)	0.744(63)	
	T_{00}	24675.783(29)	24675.68(14) ^c	
	B	0.3513(7)	0.3154(72) ^c	
$P=1f$	q	-	0.076(7) ^d	
	$a-e$	0.405(13)	0.436(60)	
	T_{00}	24675.136(50)	-	
	B	0.3069(30)	-	
$a-f$	q	-	-	
	$a-f$	0.461(32)	0.436(60)	
r.m.s		0.021	0.037	

^a Numbers in the parenthesis reflect one standard deviation of the fit.

^b Ground state constants are taken from Ref. [25].

^c Constants taken from Ref. [24]. These values are not converted (see text).

^d Constants taken from Refs. [24,25]. These values are converted (see text).

splitting parameter γ depends on the magnitude of the Renner-Teller interaction relative to the spin-orbit interaction in the $^3\Pi$ state, with a value of $0 < \gamma < 2B$.

(c) The ef components in the $P = 1$ perturber state are treated separately, to account for possible additional perturbations not included in the Hamiltonian.

We refitted the experimental data of Table 1 and find the obs. – calc. ($o - c$) values as listed. The corresponding spectroscopic parameters from this analysis are given in Table 3. The rms of the fit is $\sim 0.021 \text{ cm}^{-1}$, nearly twice as small compared to 0.037 cm^{-1} that is found when applying the previously described approach in Ref. [24]. Moreover, the two Q(2) transitions initially excluded in the fit are now reproduced as well.

The perturbations in the $\tilde{A}^1\Pi_u$ state of C_3 are more complex than described by the Hamiltonian model given in Table 2. Firstly, the origins of the $P = 1e$ and $P = 1f$ levels are found $\sim 0.65 \text{ cm}^{-1}$ apart, likely because other dark states heterogeneously perturb the e and f components of the degenerated $\tilde{A}^1\Pi_u$ and $P = 1$ states. The fluorescence lifetime measurements in Ref. [24] also show that there are at least three perturber states at the $J' = 1e$ level. Secondly, as discussed in Ref. [25], additional perturbations occurring for higher rotational levels at $J' \sim 20$ exhibit a different behavior in the e -component of the $\tilde{A}^1\Pi_u$ state. The large deviations for the $J' = 17e$ and $19e$ levels in Table 1 indicate that the effective Hamiltonian in Table 2 cannot accurately reproduce the e level energies with $J' > 17$. Further, as shown in Table 3, the derived origin of the $\tilde{A}^1\Pi_u$ state is still quite different from the value derived for high- J levels in Ref. [25]. Direct measurements of the dark perturber states as described in Ref. [26] and accurate measurements of the high- J' perturber lines are needed to perform a full deperturbation analysis of the upper $\tilde{A}^1\Pi_u$ state of $^{12}\text{C}_3$.

Even though this Hamiltonian is only an approximation, it is well applicable to analyze astronomical spectra observed in cold diffuse translucent clouds, and to derive column densities of C_3 in individual rotational levels [22]. In the latter work, it was noticed that the intensities of the R(0) and P(2) lines are slightly over-interpreted. This is also visible from Fig. 1. There are two likely reasons for this. Firstly, as discussed above, additional perturbers which could be significant for the $J' = 1$ levels are not included. Secondly, the corresponding transition intensities, which depend on the state–mixing coefficients, are very sensitive to the parameters in the Hamiltonian model. The limited number of observed transitions to the $P = 1$ perturber state, prohibits a more accurate determination of these parameters.

3.2. $^{13}\text{C}_3$

Fig. 2 shows two recorded spectra of the $\tilde{A}^1\Pi_u - \tilde{X}^1\Sigma_g^+$ electronic origin band of $^{13}\text{C}_3$ near 4051 \AA ; in trace (a) a $\sim 0.2\%$ $^{13}\text{C}_2\text{H}_2$ in He/Ar is used, in trace (b) a more diluted mixture with $\sim 0.03\%$ $^{13}\text{C}_2\text{H}_2$ is used. While the two spectra exhibit a similar number of resolved transitions, trace (a) displays a better signal-to-noise ratio, whereas trace (b) exhibits more reliable line intensities as saturation effects can be excluded. Both spectra are used for line identification and for determining accurate transition frequencies, listed in Table 4, for rotational states up to $J' = 18$.

Different from the $^{12}\text{C}_3$ spectrum, in which only transitions from *even- J'* are observed due to nuclear spin-statistics for $I(^{12}\text{C}) = 0$, all J' levels in the ground state of $^{13}\text{C}_3$ can be populated and the recorded spectra show transitions from both *even-* and *odd- J'* levels. The nuclear spin of $I(^{13}\text{C}) = 1/2$ determines a statistical weight of 1:3 for populations in *even-* and *odd- J'* levels. This intensity alternation concerning two successive rotational lines is visible in Fig. 2(b) although the intensity of some strong *odd- J'* components is slightly affected by the laser-linewidth effect. In total 16 transitions in the P-branch, 14 transitions in the Q-branch and 18 transitions in the R-branch have been observed. The assignment and transition frequencies are listed in Table 4. The experimental

Table 4

Transition frequencies (in cm^{-1}) of observed rotational lines in the $\tilde{A}^1\Pi_u - \tilde{X}^1\Sigma_g^+$ electronic origin band of $^{13}\text{C}_3$ and residuals from the fit. The frequencies of observed lines for $J' > 17$ are taken from Ref. [27] and are used after shifting to the blue by 0.08 cm^{-1} and reassigning the transitions.

J'	P-branch		Q-branch		R-branch	
	Obs.	$o - c$	Obs.	$o - c$	Obs.	$o - c$
0					24689.77	0.02
1					24690.49	0.01
2	24687.39	0.03	24688.91	0.02	24691.20	0.02
3	24686.50	0.00	24688.81	0.02	24691.85	0.01
4	24685.64	0.03	24688.69	0.04	24692.48	0.01
5	24684.71	0.02	24688.51	0.02	24693.07	0.00
6	24683.74	0.01	24688.31	0.02	24693.63	–0.01
7	24682.76	0.02	24688.09	0.02	24694.18	0.01
8	24681.72	–0.01	24687.83	0.02	24694.66	–0.02
9	24680.68	0.01	24687.52	0.01	24695.15	0.00
10	24679.59	0.00	24687.20	0.01	24695.57	–0.02
11	24678.48	0.00	24686.83	0.00	24696.00	–0.01
12	24677.33	–0.01	24686.42	–0.02	24696.37	–0.01
13	24676.17 ^a	0.00	24686.03	0.01	24696.71	–0.02
14	24674.95	–0.01			24697.02	–0.03
15	24673.72	0.00	24685.08	–0.01	24697.31	–0.02
16	24672.44	–0.02			24697.56	–0.03
17	24671.15	–0.01	24684.03	–0.01	24697.81	–0.01
18			24683.43	–0.03		
19	24668.46 ^a	–0.02	24682.84	–0.01		
20			24682.19	–0.03		
21	24665.66	–0.03	24681.55	–0.01		
22	24664.13 ^a	–0.12	24680.87	–0.01		
23	24662.87 ^a	0.08	24680.14	–0.02		
24	24661.23	–0.06	24679.41	–0.01		
25	24659.78	0.00	24678.61	–0.03		
26	24658.12 ^a	–0.11	24677.81	–0.03		
27	24656.63	–0.03	24677.01	–0.01		
28	24655.05	–0.01	24676.17 ^a	0.00		
29	24653.48	0.03	24675.28	–0.01		
30	24651.69 ^a	–0.10	24674.37	–0.01		
31	24650.23 ^a	0.10	24673.45	–0.01		
32	24648.39 ^a	–0.04	24672.50	–0.01		
33	24646.69	–0.02	24671.53	0.00	24697.73	0.05
34			24670.52	–0.01		
35	24643.21	0.01	24669.51	0.00	24697.27	0.06
36	24641.46	0.04	24668.46 ^b	0.00		
37	24639.62	0.01	24667.44	0.05	24696.68	0.03
38			24666.31	0.01		
39	24635.88	–0.05	24665.20	0.01	24696.02	0.02
40			24664.13 ^a	0.07		
41	24632.18	0.01	24662.87 ^a	–0.03	24695.25	–0.02
42			24661.74 ^a	0.01		
43	24628.33	0.01	24660.55	0.01	24694.42	–0.04
44	24626.39 ^a	0.02	24659.34	0.02		
45	24624.41	0.01	24658.12 ^a	0.03	24693.57	–0.01
46			24656.77	–0.06		
47	24620.39	–0.02	24655.56	0.00	24692.56	–0.06
48			24654.25	–0.02		
49	24616.35	0.01	24652.97	0.00	24691.55	–0.04
50			24651.69 ^a	0.05		
51	24612.21	0.01	24650.23 ^a	–0.06	24690.47	–0.02
52			24648.92	–0.01		
53	24608.02	0.03	24647.51	–0.04		
54			24646.11	–0.04		
55			24644.71	–0.03		
57			24641.82	–0.04		
59			24638.87	–0.03		
61			24635.88 ^a	0.00		
63			24632.75	–0.04		
65			24629.63	0.01		
67			24626.39 ^a	0.02		
69			24623.10	0.05		

^a Blended lines in Ref. [27].

values are further verified by comparing the ground state combination differences $R(J) - P(J + 2)$ to those derived from previously reported accurate mid-infrared $^{13}\text{C}_3$ studies [29]. The maximum deviations do not exceed 0.04 cm^{-1} for J' levels up to 17.

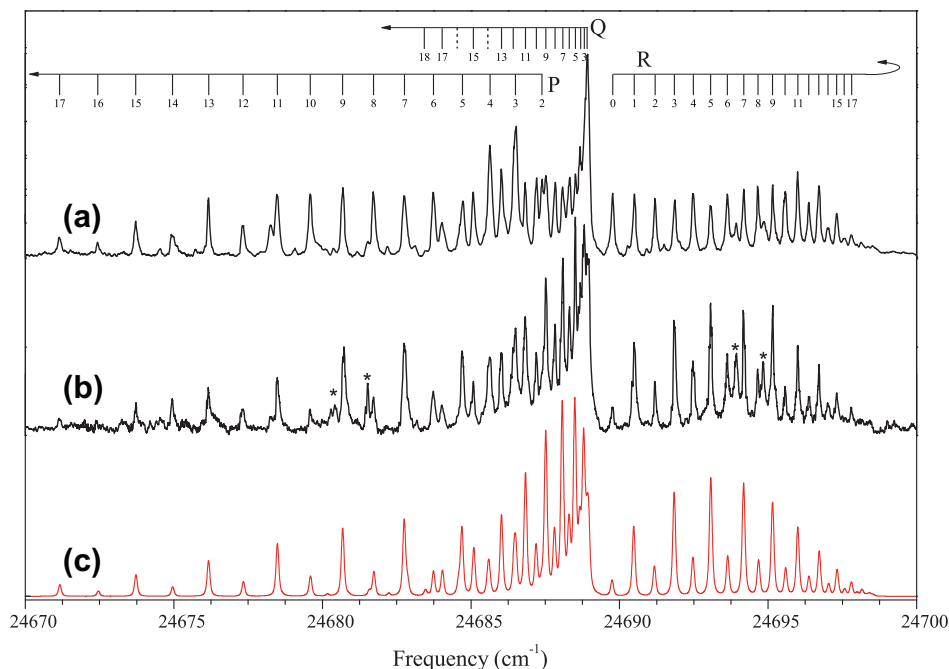


Fig. 2. Rotationally resolved spectra of the $\tilde{A}^1\Pi_u - \tilde{X}^1\Sigma_g^+$ electronic origin band of $^{13}\text{C}_3$. (a) Saturated spectrum recorded with $\sim 0.2\%$ of $^{13}\text{C}_2\text{H}_2$ in the gas mixture; (b) Spectrum recorded with $\sim 0.03\%$ of $^{13}\text{C}_2\text{H}_2$ in the gas mixture yielding reliable intensities. (c) The red trace shows the simulated spectrum for a $^1\Pi_u - ^1\Sigma_g^+$ transition, with derived constants for $^{13}\text{C}_3$, a Lorentzian width of 0.07 cm^{-1} , a Gaussian width of $\sim 0.1\text{ cm}^{-1}$, and an estimated rotational temperature of $\sim 45\text{ K}$. The lines marked with an asterisk are due to blending transitions of other small species like $^{13}\text{C}_2$ or ^{13}CH , etc. (For interpretation of the references to color in this figure legend, the reader is referred to the web version of this article.)

The emission data of the $\tilde{A}^1\Pi_u - \tilde{X}^1\Sigma_g^+$ electronic origin band of $^{13}\text{C}_3$ by Clusius and Douglas [27] add a large number of well-calibrated high- J lines to the data presented here for this band. Based on extrapolation of the molecular constants derived from the low- J levels in the CRD study, these well-resolved lines [27] are partially reassigned and subsequently included in a comprehensive analysis. It is found that the frequencies of the observed low- J transitions ($J'' < 17$) in Ref. [27] are consistent with the ones measured in the CRD spectrum when shifted $\sim 0.08\text{ cm}^{-1}$ to the blue. A consistent rotational assignment in the Q-branch is obtained upon changing the labeling of J to $J-1$ for each rotational line while the numbering of rotational lines in P- and R- branch is in agreement with our rotational assignment. The transition frequencies of the high J rotational lines presented in Ref. [27] are included in Table 4 (with reassignment where applicable).

The experimentally determined transition frequencies (Table 5) of the $^{13}\text{C}_3$ band are fitted using a standard Hamiltonian for the $\tilde{A}^1\Pi_u - \tilde{X}^1\Sigma_g^+$ transition, where the rotational energy levels in the upper $\tilde{A}^1\Pi_u$ state are represented by Eq. (2). The resulting molecular constants in the upper state fit are summarized in Table 6. The fit is carried out with the ground state constants B'' , D'' and H'' fixed to the values reported in Ref. [29], and the band origin T_{00} and upper-state B'_0 , D' , H' and q' set as variable parameters. Since the resolution of the photographed spectrum in Ref. [27] is $\sim 0.25\text{ cm}^{-1}$, uncertainties in the transition frequencies are larger than in the present experiment. Therefore, the high rotational lines ($J'' > 17$) listed in Table 5 are used with lower statistical weight in the fit by a factor of 0.5 for unblended lines and 0.3 for blended lines. A simulated spectrum using the derived molecular constants in Table 6 is shown in Fig. 2(c) and compared to the experimental spectrum shown here.

A number of features are found in the experimental spectra (marked with an asterisk) in Fig. 2(b) which do not match assignments to $^{13}\text{C}_3$ transitions. These features are not observed in the $^{12}\text{C}_2\text{H}_2/\text{He}/\text{Ar}$ plasma and thus must be due to some species con-

taining ^{13}C . As strong perturber features are observed in the spectrum of $^{12}\text{C}_3$, we considered the possibility that these features are due to an analogous perturbation in the spectrum of $^{13}\text{C}_3$. However, the deviations from the fit to a single unperturbed $^1\Pi_u - ^1\Sigma_g^+$ transition are found to be small, i.e., within their experimental uncertainties. Inspection of the observed deviations confirms that no significant perturbations for either e -parity or f -parity of high rotational levels (up to $J'' = 55$) occur in the upper $\tilde{A}^1\Pi_u$ 000 state of $^{13}\text{C}_3$. As for the observed extra lines, no pairs are found to match to ground state combination differences $R(J) - P(J+2)$ of $^{13}\text{C}_3$. The assignment of the unidentified features to other C_3 -isotopologues (e.g. $^{12}\text{C}^{13}\text{C}^{13}\text{C}$), possibly due to a small ^{12}C impurity in the precursor gas, can be excluded since the strong Q-branches of the isotopologues are not seen in Fig. 2(b). Hence, the only logical explanation for the unidentified features at this stage is that these arise from (possibly vibrationally excited) small hydrocarbon radicals that are produced in the plasma, such as $^{13}\text{C}_2$ and ^{13}CH .

3.3. ^{13}C mono- and di-substituted C_3 -isotopologues

The four partially ^{13}C -substituted $^{12}\text{C}^{13}\text{C}^{13}\text{C}$, $^{12}\text{C}^{13}\text{C}^{12}\text{C}$, $^{13}\text{C}^{12}\text{C}^{13}\text{C}$ and $^{13}\text{C}^{12}\text{C}^{12}\text{C}$ isotopologues of C_3 are systematically studied in the plasma expansion by discharging ($^{13}\text{C}_2\text{H}_2 + ^{12}\text{C}_2\text{H}_2$)/He/Ar gas mixtures with a total acetylene concentration of $\sim 0.1\%$. It is important to realize that $^{12}\text{C}_3$ and $^{13}\text{C}_3$ are produced under such plasma conditions as well, therewith adding extra transitions, but these can be distinguished based on the detailed analysis presented in the previous two sections.

Fig. 3 shows two experimental spectra recorded with typical isotope ratios of $^{12}\text{C}:^{13}\text{C} < 1$ and > 1 . The spectra are very dense. Assignments of rotational lines to a specific isotopologue and the rotational analysis of the experimental spectrum are carried out using an effective Hamiltonian for a $^1\Pi_{(u)} - ^1\Sigma_{(g)}$ transition for each ^{13}C mono- and di-substituted isotopologues as follows:

Table 5Transition frequencies (in cm^{-1}) of observed rotational lines in the $A^1\Pi-\tilde{X}^1\Sigma^+$ electronic origin band of ^{13}C mono- and di-substituted C_3 -isotopologues.

J''	P-branch		Q-branch		R-branch	
	Obs.	$o-c$	Obs.	$o-c$	Obs.	$o-c$
$^{13}\text{C}^{13}\text{C}^{12}\text{C}$						
0					24687.46 ^a	0.02
1					24688.21	0.01
2			24686.59 ^a	0.04	24688.92 ^a	-0.01
3					24689.63	0.01
4	24683.18 ^a	0.04	24686.31	0.00	24690.28	0.00
5	24682.21 ^a	0.03	24686.15	0.01	24690.93	0.03
6	24681.19	0.01	24685.94 ^a	-0.01	24691.48 ^a	-0.02
7	24680.08 ^a	-0.05	24685.70 ^a	0.00	24692.06	0.01
8			24685.43 ^a	0.01	24692.56 ^a	-0.02
9			24685.11 ^a	-0.01	24693.05 ^a	0.01
10			24684.70 ^a	-0.07	24693.50	-0.01
11			24684.41	0.02	24693.89	-0.04
12					24694.28	-0.02
13					24694.67 ^a	0.03
$^{12}\text{C}^{13}\text{C}^{12}\text{C}$						
0					24685.11 ^a	-0.02
2			24684.14 ^a	-0.04	24686.59 ^a	-0.08
4	24680.70 ^a	0.07	24683.94	-0.01	24688.04 ^a	-0.03
6	24678.60 ^a	0.01	24683.55 ^a	0.01	24689.31	-0.02
8	24676.44	0.02	24682.94 ^a	-0.07	24690.45 ^a	0.02
10			24682.38 ^a	0.04	24691.48 ^a	0.06
12			24681.47 ^a	-0.07	24692.26	0.00
$^{13}\text{C}^{12}\text{C}^{13}\text{C}$						
0					24680.73 ^a	-0.08
1					24681.47 ^a	-0.04
2			24679.96	0.02	24682.21 ^a	0.03
3			24679.85	0.00	24682.94 ^a	0.06
4					24683.55	0.04
5	24675.72	-0.01	24679.52	-0.03	24684.15 ^a	0.04
6	24674.77 ^a	-0.01	24679.37 ^a	0.02	24684.70	0.02
7	24673.79 ^a	0.01	24679.17 ^a	0.05	24685.12 ^a	-0.1
8	24672.72	-0.03	24678.85	-0.01	24685.70 ^a	-0.03
9	24671.71 ^a	-0.02	24678.60 ^a	0.03		
10	24670.62	-0.02	24678.27	0.04		
11	24669.50	-0.03				
$^{12}\text{C}^{12}\text{C}^{13}\text{C}$						
0					24678.60 ^a	0.02
1					24679.36 ^a	0.03
2			24677.72	0.03	24680.08 ^a	0.01
3			24677.60	0.02	24680.73 ^a	-0.03
4	24674.22 ^a	-0.04	24677.47	0.02	24681.47 ^a	0.05
5	24673.33	0.03	24677.31	0.02	24682.09	0.04
6	24672.35	0.03	24677.10 ^a	0.01	24682.64 ^a	-0.01
7	24671.33	0.03	24676.81 ^a	-0.04	24683.18 ^a	-0.03
8	24670.25	0.01	24676.59	0.00	24683.75 ^a	0.01
9	24669.13	-0.00	24676.29	0.00	24684.15 ^a	-0.08
10	24668.01	0.01	24675.90	-0.05	24684.70 ^a	0.01
11	24666.83	-0.02	24675.54 ^a	-0.04	24685.11 ^a	0.01
12	24665.60	-0.04	24675.20 ^a	0.03		
13	24664.40	-0.01	24674.76 ^a	0.04		
14	24663.10	-0.01				

^a Blended lines.

- (a) The approximate band origins of the four isotopologues are estimated using the previously reported band head data. Considering that the $\tilde{A}^1\Pi_u$ state of $^{12}\text{C}_3$ suffers from a strong perturbation, the isotopic shifts of the band heads with respect to $^{13}\text{C}_3$ are used instead. These have been reported in Ref. [5] to be ~ -11.0 , -9.3 , -3.9 , and -1.9 cm^{-1} for $^{12}\text{C}^{12}\text{C}^{13}\text{C}$, $^{13}\text{C}^{12}\text{C}^{13}\text{C}$, $^{12}\text{C}^{13}\text{C}^{12}\text{C}$ and $^{12}\text{C}^{13}\text{C}^{13}\text{C}$, respectively. Although not very precise, these values help to locate the band positions of the four isotopologues.
- (b) The rotational constants of the excited states of the four isotopologues are estimated by assuming that the B''_0/B'_0 ratios for the $\tilde{A}^1\Pi_u-\tilde{X}^1\Sigma^+(g)$ 000-000 band of all six C_3 -isotopologues have comparable values, i.e. ~ 1.043 , as derived for

both $^{12}\text{C}_3$ in Ref. [25] and $^{13}\text{C}_3$ in this work. Accurate values for ground state rotational constants for mono-substituted $^{12}\text{C}^{12}\text{C}^{13}\text{C}$ and $^{12}\text{C}^{13}\text{C}^{12}\text{C}$ are available from mid-infrared work [29,30] and these parameters are used throughout our study. For the ^{13}C di-substituted $^{12}\text{C}^{13}\text{C}^{13}\text{C}$ and $^{13}\text{C}^{12}\text{C}^{13}\text{C}$ isotopologues, we assume centrifugal distortion constants for both lower and upper states similar to those of $^{12}\text{C}^{12}\text{C}^{13}\text{C}$ and $^{13}\text{C}^{13}\text{C}^{13}\text{C}$.

- (c) The intensity alternations for *even-* and *odd-* J transitions due to the statistical weight of exchangeable homo-nuclear atoms are used for the assignment of the spectra of ^{13}C mono- and di-substituted isotopologues. Specifically, two of the isotopologues, $^{12}\text{C}^{13}\text{C}^{12}\text{C}$ and $^{13}\text{C}^{12}\text{C}^{13}\text{C}$, are centro-

Table 6
Spectroscopic parameters for the ^{13}C -substituted isotopologues of C_3 .^a

		$^{12}\text{C}^{12}\text{C}^{13}\text{C}$	$^{13}\text{C}^{12}\text{C}^{13}\text{C}$	$^{12}\text{C}^{13}\text{C}^{12}\text{C}$	$^{12}\text{C}^{13}\text{C}^{13}\text{C}$	$^{13}\text{C}^{13}\text{C}^{13}\text{C}$
$A^1\Pi$	T_{00}	24677.7849(53) ^a	24680.0460(63) ^a	24684.3048(93) ^a	24686.6433(69) ^a	24688.9812(46) ^a
	B'	0.39718(52)	0.38179(71)	0.4123(10)	0.39734(65)	0.3808954(20)
	$D' \times 10^6$	0.504 ^b	0.440 ^b	0.470 ^b	0.504 ^b	0.394(8)
	$H' \times 10^{11}$	–	–	–	–	5.090(17)
$\bar{X}^1\Sigma^+$	$q' \times 10^4$	–	–	–	–	2.525(41)
	B''	0.413743 ^c	0.39832(86)	0.430276 ^d	0.4143(12)	0.397024 ^e
	$D'' \times 10^6$	1.398 ^c	1.220 ^e	1.30 ^d	1.398 ^f	1.220 ^e
	$H'' \times 10^{10}$	–	–	–	–	1.05
	B''/B'	1.042	1.043	1.043	1.042	1.043

^f Estimated value from $^{12}\text{C}^{12}\text{C}^{13}\text{C}$.

^a Numbers in the parenthesis represent one standard deviation of the fit. For the band origins (T_{00}), the absolute frequency can be determined with a precision of 0.04 cm^{-1} in the present work.

^b Estimated values from the ratio of D''/D' in $^{12}\text{C}_3$.

^c Values taken from Ref. [29] and fixed.

^d Values taken from Ref. [30] and fixed.

^e Fixed to the value for $^{13}\text{C}^{13}\text{C}^{13}\text{C}$.

^f Fixed to the value for $^{12}\text{C}^{12}\text{C}^{13}\text{C}$.

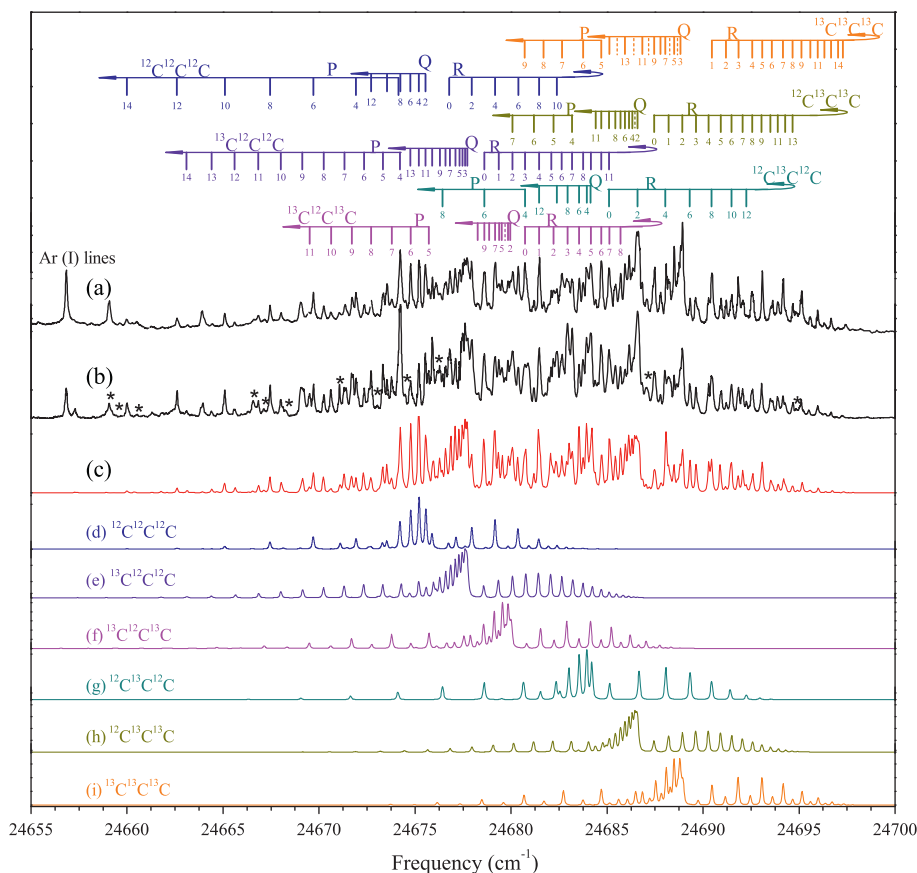


Fig. 3. The six blended spectra of the $\bar{A}^1\Pi_u - \bar{X}^1\Sigma_g^+$ 000–000 bands of the $^{12}\text{C}_3$ and ^{13}C -substituted C_3 radicals in a mixed ($^{13}\text{C}_2\text{H}_2 + ^{12}\text{C}_2\text{H}_2$)/He/Ar plasma, with (a) a ratio of $^{12}\text{C}/^{13}\text{C} < 1$ and (b) of $^{12}\text{C}/^{13}\text{C} > 1$. The Ar I absorption line [33] has been used for absolute calibration of the recorded spectra. The red trace (c) shows a weighted sum of simulated spectra, based on simulated spectra for the individual isotopologues (shown in (d–i) traces), using a Lorentzian line width of 0.07 cm^{-1} , a Gaussian line width of $\sim 0.1\text{ cm}^{-1}$, and with an estimated rotational temperature of $\sim 40\text{ K}$. The P-, Q- and R-branches of the observed rotational lines for the isotopologues are indicated. The lines marked with an asterisk are due to blending transitions of other small species or unknown perturbation features. (For interpretation of the references to color in this figure legend, the reader is referred to the web version of this article.)

symmetric linear molecules and their spectra will show intensity alternations. In the case of $^{12}\text{C}^{13}\text{C}^{12}\text{C}$ with two identical ^{12}C atoms with $l=0$, only *even- J* transitions can be observed in the spectrum, while in the case of $^{13}\text{C}^{12}\text{C}^{13}\text{C}$ with two identical ^{13}C atoms with $l=1/2$, an intensity alternation with a statistical weight of 1:3 for *even-* and *odd- J* transitions occurs, respectively.

In total, 35 transitions are assigned to $^{12}\text{C}^{12}\text{C}^{13}\text{C}$, 24 to $^{13}\text{C}^{12}\text{C}^{13}\text{C}$, 16 to $^{12}\text{C}^{13}\text{C}^{12}\text{C}$, and 27 to $^{12}\text{C}^{13}\text{C}^{13}\text{C}$. The transition frequencies are listed in Table 5. The rotational assignment for each transition is indicated in Fig. 3 for all isotopologues. A zoomed-in portion of the cumulative spectrum is shown in Fig. 4.

Least-squares fits are performed based on the experimental transition frequencies for each of the isotopologues, where the fre-

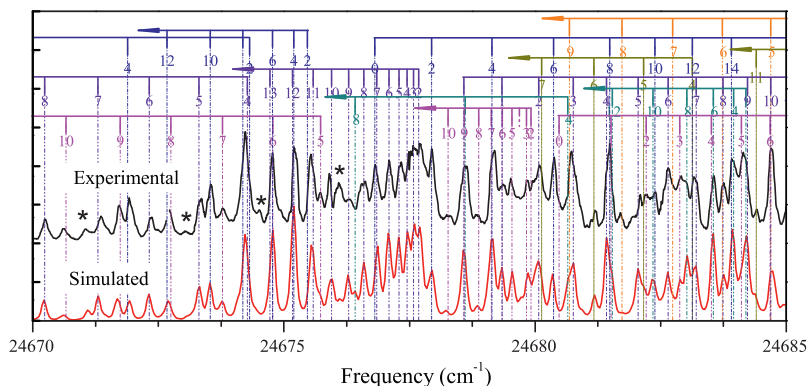


Fig. 4. A zoomed-in plot of Fig. 3. The black trace shows the observed spectrum through the mixed ($^{13}\text{C}_2\text{H}_2 + ^{12}\text{C}_2\text{H}_2$)/He/Ar plasma, with ratio $^{12}\text{C}/^{13}\text{C} < 1$ and the red trace shows the weighted sum of the simulated spectra (lower trace) using the estimated relative concentrations of all individual isotopologues. The P-, Q- and R-branch transitions are indicated using the calculated values. The lines marked with an asterisk are due to other small species or unknown perturbation features. (For interpretation of the references to color in this figure legend, the reader is referred to the web version of this article.)

frequencies of blended lines are included with a lower statistical weight in the fits. Similar as for $^{13}\text{C}_3$, a standard $^1\Pi - ^1\Sigma^+$ Hamiltonian is used for all four partially substituted isotopologues. For the mono-substituted $^{12}\text{C}^{12}\text{C}^{13}\text{C}$ and $^{12}\text{C}^{13}\text{C}^{12}\text{C}$, the band origins T_{00} and upper-state constants B'_0 and D' are set as variable parameters while the ground state constants B''_0 , D'' are fixed to the values available from previous mid-infrared work [29,30]. Considering that only a limited number of low- J transitions are observed in our spectra, this does not allow for determining Λ -type doubling constants q' and centrifugal distortion constants D' ; values for D' and q' are therefore kept fixed in the fits in which D' has been estimated from the D''/D' ratio of $^{12}\text{C}_3$ [25] and q' is fixed at 0. For the di-substituted $^{13}\text{C}^{12}\text{C}^{13}\text{C}$ and $^{12}\text{C}^{13}\text{C}^{13}\text{C}$, for which ground state constants are not available, the centrifugal distortion constants are fixed to those of $^{13}\text{C}^{13}\text{C}^{13}\text{C}$ and $^{12}\text{C}^{12}\text{C}^{13}\text{C}$. The ground state and upper state rotational constants B'' and B' and the band origins T_{00} follow from the fit.

The resulting spectroscopic constants are summarized in Table 6. A simulated sum spectrum, Fig. 3(c) and simulated individual spectrum for each isotopologue (Fig. 3(d)–(i)) using the parameters given in Table 6, are shown and compared to the experimental spectrum. The simulated spectra shown in Fig. 3 (and Fig. 4) take into account the statistical abundance and estimated concentration of each C_3 isotopologue produced in the plasma. A few weak features are observed, marked by asterisks in Figs. 3 and 4 that could not be assigned to any C_3 -isotopologues and are likely due to other small hydrocarbon radicals.

For the four centro-symmetric C_3 isotopologues ($^{12}\text{C}^{12}\text{C}^{12}\text{C}$, $^{12}\text{C}^{13}\text{C}^{12}\text{C}$, $^{13}\text{C}^{12}\text{C}^{13}\text{C}$ and $^{13}\text{C}^{13}\text{C}^{13}\text{C}$) the derived rotational constants can be used to estimate the values of the effective CC bond lengths, assuming that for such a geometry the two bonds are identical for each configuration. Such procedure yields consistent values of effective bond lengths for all the four isotopologues: 1.277(2) Å in the $\tilde{X}^1\Sigma_g^+$ (000) state, and 1.303(3) Å in the $\tilde{A}^1\Pi_u$ (000) state. The two values are also found to reasonably reproduce the rotational constants (B'_0 , B''_0) of the other two isotopologues ($^{12}\text{C}^{12}\text{C}^{13}\text{C}$ and $^{12}\text{C}^{13}\text{C}^{13}\text{C}$) as listed in Table 6, with deviations less than 0.1%. The present data do not allow to derive more accurate values. A direct comparison of the experimental values with theoretical equilibrium values is challenging, given the highly flat character of the potential surface in the ground state [1] and the double-minimum asymmetric stretching potential surface in the $\tilde{A}^1\Pi_u$ state [1,43]. In parallel, the multiple and severe perturbations in the $\tilde{A}^1\Pi_u$ state of $^{12}\text{C}_3$ should also be taken into account. Therefore, more and more precise measurements are needed to derive highly accurate molecular geometries from this type of data.

4. Conclusion

In the present study high resolution spectra are presented for the $\tilde{A}^1\Pi_u - \tilde{X}^1\Sigma_g^+$ 000–000 band of all six ^{12}C and ^{13}C containing isotopologues of the C_3 molecule. Pure spectra have been recorded for $^{12}\text{C}_3$ and $^{13}\text{C}_3$ and partially overlapping spectra of the mixed isotopologues have been unraveled. Molecular constants for the $\tilde{A}^1\Pi_u$ excited state have been determined. For $^{13}\text{C}^{12}\text{C}^{13}\text{C}$ and $^{12}\text{C}^{13}\text{C}^{13}\text{C}$ also the ground state constants have been determined for the first time.

The perturbation in $^{12}\text{C}_3$ has been analyzed thoroughly in Ref. [24] and [25]. In the present work we have adapted the effective Hamiltonian model describing the $\tilde{A}^1\Pi_u - \tilde{X}^1\Sigma_g^+$ 000–000 band of $^{12}\text{C}_3$, specifically to interpret recent astronomical observations of interstellar C_3 [22]. Despite the fact that our model does not work well for high- J transitions, it can be used to reproduce line positions and intensities of low- J transitions of $^{12}\text{C}_3$ reasonably well, with inclusion of the Q(2) lines. In contrast to $^{12}\text{C}_3$, no perturbation is found for $^{13}\text{C}_3$ in the $\tilde{A}^1\Pi_u$ 000 state even up to very high J -levels, including data of Clusius and Douglas [27]. This results in accurate effective constants in the $\tilde{A}^1\Pi_u$ state of $^{13}\text{C}_3$. Also for the $\tilde{A}^1\Pi_u$ state of ^{13}C -mono and di-substituted isotopologues no clear evidence for perturbations is found.

C_3 is the largest carbon chain species identified so far in the diffuse interstellar medium. The astronomical detection of a ^{13}C -substituted isotopologue (and resulting isotope ratio) therefore may be useful as a diagnostic tool to monitor the physical and chemical processes taking place in the diffuse interstellar medium, similar to previous studies on CH^+ and CN [44–46]. The corresponding spectrum will be largely covered by that of the main isotopologue, as the relative intensities reflecting the isotope abundances. An unambiguous identification will become only possible for observations with sufficient resolution to distinguish the individual species. We have compared the simulated spectra of two ^{13}C mono-substituted isotopologues, i.e., the spectra shown in Fig. 3(e) and (g), to the astronomical spectra towards HD 169454 as presented in Ref. [22]. This does not provide convincing evidence for a positive identification of $^{13}\text{C}^{12}\text{C}^{12}\text{C}$ and $^{12}\text{C}^{13}\text{C}^{12}\text{C}$. Astronomical data with higher spectral resolution are needed for this.

Acknowledgments

We thank Prof. Thomas Giesen (Cologne/Kassel) for generously providing us with spectroscopic constants of several C_3 isotopo-

logues, prior to publication. We are indebted to an anonymous reviewer who has provided important suggestions to improve this manuscript. We furthermore acknowledge financial support by FOM, NOVA and the 'Stichting Physica'. This work has been performed as part of ongoing research within the Dutch Astrochemistry Network.

References

- [1] M. Mladenovic, S. Schmatz, P. Botschwina, *J. Chem. Phys.* 101 (1994) 5891–5899.
- [2] K. Ahmed, G.G. Balint-Kurti, C.M. Western, *J. Chem. Phys.* 121 (2004) 10041–10051.
- [3] W. Huggins, *Proc. R. Soc. London* 33 (1882) 1.
- [4] G. Herzberg, *Astrophys. J.* 96 (1942) 314–315.
- [5] A.E. Douglas, *Astrophys. J.* 114 (1951) 466–468.
- [6] L. Gausset, G. Herzberg, B. Rosen, A. Lagerqvist, *Discuss. Faraday Soc.* 35 (1963) 113–117.
- [7] L. Gausset, G. Herzberg, A. Lagerqvist, B. Rosen, *Astrophys. J.* 142 (1965) 45–76.
- [8] A.G.G.M. Tielens, *The Physics and Chemistry of the Interstellar Medium*, Cambridge University Press, 2005.
- [9] R.I. Kaiser, *Chem. Rev.* 102 (2002) 1309–1358.
- [10] J. Cernicharo, J.R. Goicoechea, E. Caux, *Astrophys. J.* 534 (2000) L199–L202.
- [11] K.W. Hinkle, J.J. Keady, P.F. Bernath, *Science* 241 (1988) 1319–1322.
- [12] B. Mookerjee et al., *Astron. Astrophys.* 521 (2010) L13.
- [13] T.F. Giesen, A.O. Van Orden, J.D. Cruzan, R.A. Provencal, R.J. Saykally, R. Gendriesch, F. Lewen, G. Winnewisser, *Astrophys. J.* 551 (2001) 181–184; T.F. Giesen, A.O. Van Orden, J.D. Cruzan, R.A. Provencal, R.J. Saykally, R. Gendriesch, F. Lewen, G. Winnewisser, *Astrophys. J.* 555 (2001) L77. Erratum.
- [14] K. Matsumura, H. Kanamori, K. Kawaguchi, E. Hirota, *J. Chem. Phys.* 89 (1988) 3491–3494.
- [15] K. Kawaguchi, K. Matsumura, H. Kanamori, E. Hirota, *J. Chem. Phys.* 91 (1989) 1953–1957.
- [16] C.A. Schmuttenmaer, R.C. Cohen, N. Pugliano, J.R. Heath, A.L. Cooksy, K.L. Busarow, R.J. Saykally, *Science* 249 (1990) 897–900.
- [17] J.P. Maier, N.M. Lakin, G.A.H. Walker, D.A. Bohlender, *Astrophys. J.* 553 (2001) 267–273.
- [18] E. Roueff, P. Felenbok, J.H. Black, C. Gry, *Astron. Astrophys.* 384 (2002) 629–637.
- [19] G. Galazutdinov, A. Petlewski, F. Musaeu, C. Moutou, G. Curto Lo, J. Krelowski, *Astron. Astrophys.* 395 (2002) 969–974.
- [20] M. Ádámkóvics, G.A. Blake, B.J. McCall, *Astrophys. J.* 595 (2003) 235–246.
- [21] T. Oka, J.A. Thorburn, B.J. McCall, S.D. Friedman, L.M. Hobbs, P. Sonnentrucker, D.E. Welty, D.G. York, *Astrophys. J.* 582 (2003) 823–829.
- [22] M. Schmidt, J. Krelowski, G. Galazutdinov, D. Zhao, M.A. Haddad, W. Ubachs, H. Linnartz, *Mon. Not. R. Astron. Soc.*, Submitted.
- [23] B.J. McCall, R.N. Casaes, M. Ádámkóvics, R.J. Saykally, *Chem. Phys. Lett.* 374 (2003) 583–586.
- [24] G.Q. Zhang, K.S. Chen, A.J. Merer, Y.C. Hsu, W.J. Chen, S. Shaji, Y.A. Liao, *J. Chem. Phys.* 122 (2005) 244308.
- [25] A. Tanabashi, T. Hirao, T. Amano, P.F. Bernath, *Astrophys. J.* 624 (2005) 1116–1120.
- [26] Y. Sych, P. Bornhauser, G. Knopp, Y. Liu, T. Gerber, R. Marquardt, P.P. Radi, *J. Chem. Phys.* 139 (2013) 154203.
- [27] K. Clusius, A.E. Douglas, *Can. J. Phys.* 32 (1954) 319–325.
- [28] W. Weltner, D. McLeod, *J. Chem. Phys.* 40 (1964) 1305–1316.
- [29] N. Moazzen-Ahmadi, A.R.W. McKellar, *J. Chem. Phys.* 98 (1993) 7757–7762.
- [30] J. Krieg, V. Lutter, C.P. Endres, I.H. Keppeler, P. Jensen, M.E. Harding, J. Vázquez, S. Schlemmer, T.F. Giesen, S. Thorwirth, *J. Phys. Chem. A* 117 (2013) 3332–3339.
- [31] D. Zhao, M.A. Haddad, H. Linnartz, W. Ubachs, *J. Chem. Phys.* 135 (2011) 044307.
- [32] T. Motylewski, H. Linnartz, *Rev. Sci. Instrum.* 70 (1999) 1305–1312.
- [33] A. Kramida, Yu. Ralchenko, J. Reader and NIST ASD Team, *NIST Atomic Spectra Database (ver. 5.1)*, National Institute of Standards and Technology, Gaithersburg, 2013.
- [34] R.T. Jongma, M.G.H. Boogaarts, I. Holleman, G. Meijer, *Rev. Sci. Instrum.* 66 (1995) 2821–2828.
- [35] M.A. Haddad, D. Zhao, H. Linnartz, W. Ubachs, *Chinese J. Chem. Phys.* 25 (2012) 129–134.
- [36] N. Wehres, D. Zhao, W. Ubachs, H. Linnartz, *Chem. Phys. Lett.* 497 (2010) 30–32.
- [37] H. Lefebvre-Brion, R.W. Field, *The Spectra and Dynamics of Diatomic Molecules*, Elsevier, Amsterdam, 2004.
- [38] PGOPHER, a Program for Simulating Rotational Structure, C. M. Western, University of Bristol, <<http://pgopher.chm.bris.ac.uk>>.
- [39] A.J. de Nijs, E.J. Salumbides, K.S.E. Eikema, W. Ubachs, H.L. Bethlem, *Phys. Rev. A* 84 (2011) 052509.
- [40] D.W. Tokaryk, S. Civis, *J. Chem. Phys.* 103 (1995) 3928–3941.
- [41] L. Veseth, *Can. J. Phys.* 53 (1975) 299–302.
- [42] J.T. Hougen, *J. Chem. Phys.* 36 (1962) 1874–1881.
- [43] M. Izuha, K. Yamanouchi, *J. Chem. Phys.* 109 (1998) 1810–1818.
- [44] S. Casassus, O. Stahl, T.L. Wilson, *Astron. Astrophys.* 441 (2005) 181–194.
- [45] C. Savage, A.J. Apponi, L.M. Ziurys, S. Wyckoff, *Astrophys. J.* 578 (2002) 211–223.
- [46] O. Stahl, S. Casassus, T. Wilson, *Astron. Astrophys.* 477 (2008) 865–875.